

Quantum chaotic patterns and clustering in spectra of a two-level boson model

Eva Majerníková, and S. Shpyrko[†]

*Institute of Physics, Slovak Academy of Sciences,
Dúbravská cesta 9, SK-84 511 Bratislava, Slovak Republic*
and

*Department of Theoretical Physics, Palacký University,
Tr. 17. listopadu 50,
CZ-77207 Olomouc, Czech Republic*

[†] *Institute for Nuclear Research,
Ukrainian Academy of Sciences,
pr. Nauki 47, 03068 Kiev, Ukraine*

We studied excited spectra of a two level system coupled to two phonon (vibron) modes represented by Jahn-Teller model. In the rotation symmetric version ($E \otimes e$ model) for particular rotation quantum numbers, a coexistence of (i) two types of dimerized regions, namely long-range ordered (extended) dimerized pairs of oscillating levels and a short-range ordered (localized) "kink lattice" of avoided levels, and of (ii) an intermediate region of kink nucleation with variable range of ordering was found. This structure appears above certain critical line as function of interaction strength. Dimerization level clustering and level avoiding generic patterns reflect themselves in several intermittent regions between up-to three branches of spectral entropies as well as in peculiarities of partial (given quantum angular momentum) as well as cumulative level spacing probability distributions. The clustering of level spacings causes drastic differences from the Poisson distribution. Linear scaling behavior of the widths of curvature probability distributions provides an indication of patterns of quantum chaos in the system. In the quasiclassical limit we have found local chaotic regime in phonon frequency spectra at intermediate energies, strong dependence of sample phonon trajectories on initial conditions and existence of separatrices between several domains of their chaotic motion.

PACS numbers: 31.30.-i, 63.22.+m, 05.45.Mt

I. INTRODUCTION

Generally, multitude of avoided crossings in complex spectra of a quantum system is considered as being a pattern for manifestation of chaos in a quasiclassical limit of nonlinear many body systems with repulsive interactions^{1,2,3,4,5,6}. Numerical investigations of excited spectra of certain two-level systems coupled to bosons (e.g., exciton model^{7,8}, $E \otimes e$ Jahn-Teller model⁹) show existence of level avoidings and of related "exotic" (localized) states. Various aspects of quantum chaotic patterns of two-level systems coupled to bosons still remain objects of interest since the early studies of atoms coupled to a boson mode, e.g. exciton and Jaynes-Cummings models^{3,4,5,10,11}. In solid state physics, quantum chemistry or in quantum optics the chaos bearing models are of special relevance for understanding, e.g., their optical and transport properties. The effect of chaos in excited spectra can be analogous to effects related with Anderson localization in solids. For a two-degrees-of freedom harmonic oscillator Berry et al¹² have found level clustering and level avoidings resulting from strong kinematical repulsions and therefore certain deviations of the level spacing distribution from the Poissonian one.

In the present paper we investigate a class of quantum dynamical two-level Hamiltonian of $SU(2)$ symmetry coupled with two boson modes of different parity whose familiar representative is Jahn-Teller model. (Analogous investigations can be done also for the case of exciton coupled to one boson mode).

Recently, Yamasaki et al¹³ investigated existence of chaos in dynamical $E \otimes e$ Jahn-Teller (JT) model¹⁴. Their analysis was based on separation the adiabatic "mexican hat" potential and an additional anharmonic part supplemented via a parameter for a nonlinear mode coupling of trigonal symmetry to include the effect of fluctuations and nonintegrability. The nonlinearity was included via mode coupling in addition to the mean field bare part of the Hamiltonian. The authors concluded the existence of quantum chaotic patterns of the investigated system to be a consequence of the said nonlinearity of the Hamiltonian, meanwhile for the linear part the conclusion was made about the absence of these patterns.

Our system under investigation differs from the said system in the following: a) we *do not* introduce explicitly nonlinearity in the initial Hamiltonian. However, $SU(2)$ symmetry of the system involves *intrinsic nonlinearity* which can be made revealed by exact elimination of the electronic degrees of freedom and renders place for interesting patterns of chaotic origin; b) We start from the generalized $E \otimes (b_1 + b_2)e$ model, the symmetric $E \otimes e$ model presenting its particular case with equal coupling constants and with symmetry of higher (rotational) symmetry group. As we pointed out in our preceding paper¹⁵, the difference of coupling constants in realistic systems is likely to be caused, for example, by spatial anisotropy of crystals. Variational approach to the generalized model used for calculation of the ground state presented in¹⁵ was shown to yield the biggest discrepancies for the rotation symmetric case. We have found

that in the ground state the abrupt change of behavior of the energy at equal couplings is an artefact of the adiabatic approximation: the energy region of the quantum $E \otimes e$ model is situated within a smeared boarder at $\chi \equiv \beta/\alpha = 1$ between the "selftrapping" and "tunnelling" part of the ground state of the model with broken rotational symmetry as a function of the symmetry breaking parameter χ . In this transition region both phases coexist and are quantum correlated via nonlinear correlations between the modes. There the overlapping interaction contribution to the energy from the admixture of two levels (in the excitation reflection Ansatz for variational wave function) causes a dramatic decrease of the ground state energy because of reflection operator changing parity (the mechanism seems to be of general validity for two-level models¹⁶). The same effect is expected to participate also in excited spectrum. Related decrease of energy will not only compensate the increase of the unperturbed energy $E_n^0 \rightarrow E_{n+1}^0$ but cause even the net decrease of the energy due to the overlapping of respective excited wave functions and resulting in a tunneling-flip (kink) to continue at the next level when increasing the coupling constant (This mechanism can be well recognized, e.g., in Figs. 1b,d). The tunneling mechanism can be demonstrated also within the Calogero-Moser formalism of many pseudoparticles with repulsive interaction^{17,18} (Section III).

For the present investigations we shall concentrate (both from Hamiltonian and statistical point of view) mainly on the symmetric JT case, whereas the generalized case is to be the subject of a subsequent contribution¹⁹.

In the Section II we present analytical formulation of the eigenvalue problem of the generalized Jahn-Teller Hamiltonian in radial coordinates with the radial symmetry breaking term. In the representation with definite parity and square of angular momentum we investigate numerically respective excited phonon wave functions and energy spectra of the rotational symmetric version of the model.

In the Section III we present approximate analytical approaches to the symmetric JT model in the strong and weak coupling limits in order to elucidate peculiar features of the excited spectra. Special interest is given to identification of regions of the spectra with different extent of ordering, from long-range ordered region (extended states) to short range ordering of localized states with dynamical avoiding.

In the Section IV we consider a proper semiclassical limit of the JT system. In support to the searched patterns of quantum classical behavior we showed that its semiclassical counterpart is able of bearing chaotic motion in mediate intervals of energies. Within the domain of the chaotic motion we indicate also the existence of pronounced separatrices in the phase space plane which divide several nonoverlapping regions.

In the Section V we calculate the nearest level spacing probability distributions used generally in investi-

gations of complex spectra as the relevant statistical characteristics^{1,2}. As the most informative were found particular level spacing distributions for separate rotation quantum numbers. The scaling function of the widths of probability distributions of level curvatures was shown to satisfy a criterion for the existence of chaos in the semiclassical limit²⁰. It is indicated also that for small values of couplings there are serious deviations from the expected Poisson statistics of the nearest-neighbor distributions for the cumulative (taken for all j) picture of energy levels.

II. HAMILTONIAN AND EQUATIONS FOR EXCITED SPECTRUM

We investigate local spinless double degenerate electron states linearly coupled to two intramolecular phonon (vibron) modes described by Hamiltonian

$$H = \Omega(b_1^\dagger b_1 + b_2^\dagger b_2 + 1)I + \alpha(b_1^\dagger + b_1)\sigma_z - \beta(b_2^\dagger + b_2)\sigma_x, \quad (1)$$

where $\sigma_x = \begin{pmatrix} 0 & 1 \\ 1 & 0 \end{pmatrix}$, $\sigma_y = i \begin{pmatrix} 0 & -1 \\ 1 & 0 \end{pmatrix}$, $\sigma_z = \begin{pmatrix} 1 & 0 \\ 0 & -1 \end{pmatrix}$ are Pauli matrices, I is the unit matrix. This pseudospin notation refers to two-level electronic system, the Hamiltonian is thus 2×2 matrix.

For general $\alpha \neq \beta$ the Hamiltonian possesses a special $SU(2)$ symmetry with the reflection operator \hat{R} acting on phonon and electron subspace:

$$\hat{R} = R_{el}R_{ph}, \quad R_{el} = \sigma_x, \quad R_{ph} = \exp(i\pi b_1^\dagger b_1) \quad (2)$$

and $R_{ph}Q_1 = -Q_1R_{ph}$, $R_{ph}Q_2 = Q_2R_{ph}$. Thus we have: $[R, H] = 0$ and the eigenstates of the problem can be cast as the eigenfunctions of the reflection operator with eigenvalues ± 1 which are good quantum numbers.

If $\alpha = \beta$, the Hamiltonian becomes rotationally symmetric in the plane ($Q_1 \times Q_2$) and there arises another "good" quantum number, namely the eigenvalue of angular momentum \hat{J} which in fact is nothing but the infinitesimal generator of the rotational group:

$$\hat{J} = i(b_1 b_2^+ - b_1^+ b_2) - \frac{1}{2}\sigma_y. \quad (3)$$

Therefore, in the vicinity of the symmetric JT case it is feasible to cast the solutions in the form respecting this rotational symmetry.

To account accurately for group properties of the Hamiltonian we introduce radial coordinates in the $Q_1 \times Q_2$ plane $Q_1 = r \cos \phi$, $Q_2 = r \sin \phi$.

The angular momentum operator is therefore

$$\hat{J} = -i \frac{\partial}{\partial \phi} - \frac{1}{2}\sigma_y, \quad (4)$$

and that of the reflection

$$\hat{R} = R_{el} \cdot R_{ph}(r, \phi), \quad (5)$$

where the phonon part of the reflection operator acts as $R_{ph}(r, \phi)f(r, \phi) = f(r, \pi - \phi)$ for some $f(r, \phi)$ affecting only ϕ coordinate. The eigenfunctions of the angular momentum operator with eigenvalue j (i.e., $\hat{J}\Psi = j\Psi$) can be cast as follows:

$$\Psi_j = f_1(r) \cdot |+\rangle e^{i\phi(j-\frac{1}{2})} + f_2(r) \cdot |-\rangle e^{i\phi(j+\frac{1}{2})}, \quad (6)$$

with arbitrary $f_1(r), f_2(r)$ to be determined below. Electronic wavefunctions are expressed as

$$|+\rangle = \frac{1}{2} \begin{pmatrix} 1+i \\ 1-i \end{pmatrix}, \quad |-\rangle = \frac{1}{2} \begin{pmatrix} 1-i \\ 1+i \end{pmatrix}.$$

The angular quantum number j takes on the values $j = \pm 1/2, \pm 3/2, \pm 5/2, \dots$. The operator \hat{J} does not commute with the reflection operator \hat{R} , but \hat{J}^2 does, so it is more convenient to build solutions as joint eigenfunctions of \hat{R} and \hat{J}^2 rather than \hat{J} .

In order to make use of the reflection property of the Hamiltonian we perform the custom Fulton-Gouterman transformation²¹ by means of the operator U :

$$U = \frac{1}{\sqrt{2}} \begin{pmatrix} 1, R_{ph} \\ 1, -R_{ph} \end{pmatrix}. \quad (7)$$

The resulting Hamiltonian is diagonal in electronic space and is represented in its full form as follows:

$$\begin{aligned} \tilde{H} \equiv \hat{U}\hat{H}\hat{U}^{-1} = & \left[-\frac{1}{2r} \frac{\partial}{\partial r} \left(r \frac{\partial}{\partial r} \right) + \frac{1}{2} r^2 \right] - \frac{1}{2r^2} \cdot \frac{\partial^2}{\partial \phi^2} \\ & + \sqrt{2}\alpha r \cdot \begin{pmatrix} \cos \phi - \sin \phi R_{ph} & 0 \\ 0 & \cos \phi + \sin \phi R_{ph} \end{pmatrix} \\ & + (\alpha - \beta)\sqrt{2}r \cdot \begin{pmatrix} \sin \phi R_{ph} & 0 \\ 0 & -\sin \phi R_{ph} \end{pmatrix}, \end{aligned} \quad (8)$$

where R_{ph} (2) is the (highly nonlinear) phonon reflection operator in the radial coordinates, which affects now only the ϕ coordinate. In Equation (8) we extracted explicitly the last term $\sim (\alpha - \beta)$ which breaks the rotational symmetry of the problem. Just for reference we mention the corresponding transformation of the angular momentum and its square:

$$\tilde{J} = -i \frac{\partial}{\partial \phi} \sigma_x + \frac{1}{2} \sigma_y R_{ph}. \quad (9)$$

$$\tilde{J}^2 = \left(-\frac{\partial^2}{\partial \phi^2} + \frac{1}{4} \right) + \frac{\partial}{\partial \phi} \sigma_z R_{ph}, \quad (10)$$

The transformed electron reflection operator is of course, trivial *per constructionem*, $\tilde{R}_{el} = \sigma_z$.

Although the E \otimes e JT case ($\alpha = \beta$) was solved by Longuet-Higgins et al²² long time ago, we present briefly the solution using another representation of the states, which enables us to distinguish the "ordered" and "exotic" states, as we explain in Section III. The case $\alpha \neq \beta$ can be included on equal footing. The wavefunctions we are concerning with have definite parity ± 1 and definite square of angular momentum j^2 . Let us set $K = \exp(i\pi(j - 1/2)) = \pm 1$.

1) In the case $K = +1$ (or $j - 1/2 = 0, 2, 4, 6, \dots; -2, -4, \dots$) the *gerade* solutions read as

$$\tilde{\Psi} = \begin{pmatrix} 1 \\ 0 \end{pmatrix} \left\{ f_1(r) \cdot \frac{1}{2\pi} \left[\sin \left(j - \frac{1}{2} \right) \phi - \cos \left(j - \frac{1}{2} \right) \phi \right] + f_2(r) \cdot \frac{1}{2\pi} \left[\sin \left(j + \frac{1}{2} \right) \phi - \cos \left(j + \frac{1}{2} \right) \phi \right] \right\} \quad (11)$$

We shall refer to the angular wavefunction in both square brackets correspondingly as $|\pm\rangle$ or Φ_j^\pm .

2) In the case $K = -1$ (or $j - 1/2 = 1, 3, 5, 7, \dots; -1, -3, \dots$) we have the expression similar to (11) but with the "−" signs in both square brackets.

The *ungerade* case can be recovered if one takes the vector $\begin{pmatrix} 0 \\ 1 \end{pmatrix}$ instead of $\begin{pmatrix} 1 \\ 0 \end{pmatrix}$. We limit ourselves to the case of *gerade* parity, that is in the representation (8) we are to take the upper row of the matrices only.

The secular equations for the vibronic part (functions $f_1(r), f_2(r)$) in both cases are

$$H_r f_1 + \frac{1}{2r^2} \left(j - \frac{1}{2} \right)^2 f_1 + \alpha\sqrt{2}r f_2 = E f_1 \quad (12)$$

$$H_r f_2 + \frac{1}{2r^2} \left(j + \frac{1}{2} \right)^2 f_2 + \alpha\sqrt{2}r f_1 = E f_2, \quad (13)$$

where the radial part H_r is

$$H_r = -\frac{1}{2r} \frac{\partial}{\partial r} \left(r \frac{\partial}{\partial r} \right) + \frac{1}{2} r^2. \quad (14)$$

In the case $\alpha = \beta = 0$ the problem is exactly that of two independent oscillators and its solution in terms of the special functions is well-known. Thus, the solutions are grouped according to the $|j|$ value ($j = 1/2, 3/2, 5/2, \dots$; the parity is $+1$, as before). Within the same j the functions are divided into two groups:

a) States with $f_2 = 0$ and

$$f_1 \equiv \Phi^{(+)}(n_r, j; r) = \frac{1}{\sqrt{C_{n_r, j}^+}} \exp\left(-\frac{r^2}{2}\right) \cdot r^{|j-\frac{1}{2}|} \cdot {}_1F_1\left(-n_r, 1 + \left|j - \frac{1}{2}\right|, r^2\right), \quad (15)$$

where n_r ("radial" quantum number) takes positive integer values $n_r = 0, 1, 2, \dots$; ${}_1F_1(a, b, z)$ is a confluent hypergeometric function (satisfying equation $zy'' + (b - z)y' - ay = 0$), and the norm is

$$\frac{1}{C_{n_r, j}^+} = \frac{(|j - \frac{1}{2}|)!}{2} \cdot \frac{1}{C_{|j - 1/2|}^{n_r + |j - 1/2|}} \quad (16)$$

(here $C_m^n \equiv n!/[m!(n - m)!]$ is a common combinatorial factor). These states we label as $|+\rangle$ -states (they correspond to the $|+\rangle$ -function of angular momentum). The product of two radial functions is defined as $\int_0^\infty r \Phi_{n_r, j}^\pm \Phi_{n_r, j}^\pm dr$. The energy spectrum is $E^+ = 2n_r + |j - \frac{1}{2}| + 1$, and the "main" quantum number is therefore $n = 2n_r + |j - 1/2|$.

b) States with $f_1=0$ and $f_2 \equiv \Phi^{(-)}(n_r, j; r)$ given by the same expression as (15) but with $j + 1/2$ instead of $j - 1/2$. We refer to these states as $|-\rangle$ -states.

The mentioned two groups correspond to two initially degenerate electron levels; these states are coupled together by means of the strongly nonlinear transformation involving the reflection operator $R(r, \phi)$, thus the situation is similar to the FG treatment in ordinary phonon

coordinates, where the nonlinear reflection operator coupled the states pertaining to lower and upper electron level.

Writing secular equations for the problem with $\alpha \neq 0$ is straightforward. The solution is sought as $f_1 = \sum_{n_r} a_{n_r} \Phi_{n_r}^+$, $f_2 = \sum_{n_r} b_{n_r} \Phi_{n_r}^-$, or, in unified notations $f = \sum_{n=0}^\infty c_n \Phi_n$, where $\{c_n\} \equiv \{a_0, b_0, a_1, b_1, a_2, b_2, a_3, \dots\}$, and

$$\Phi_n = \begin{cases} \Phi^+(n_r, j), & n = 2n_r, \\ \Phi^-(n_r, j), & n = 2n_r + 1. \end{cases} \quad (17)$$

The only non-zero off-diagonal elements are

$$f_{n_r n_r} \equiv \sqrt{2} \int \Phi_{n_r}^+ \Phi_{n_r}^- r \cdot r dr = \sqrt{2} \sqrt{n_r + 1 + |j - \frac{1}{2}|} \quad (18)$$

$$f_{n_r + 1 n_r} \equiv \sqrt{2} \int \Phi_{n_r + 1}^+ \Phi_{n_r}^- r \cdot r dr = -\sqrt{2} \sqrt{n_r + 1} \quad (19)$$

Therefore, secular equation acquires the famous tridiagonal form ($E^{(0)}$ is "unperturbed" energy for corresponding n, j),

$$c_n E_n^{(0)} + \alpha(c_{n+1} f_{n_r n_r} + c_{n-1} f_{n_r n_r - 1}) = E c_n, \quad n = 2n_r, \quad (20)$$

$$c_n E_n^{(0)} + \alpha(c_{n-1} f_{n_r n_r} + c_{n+1} f_{n_r + 1 n_r}) = E c_n, \quad n = 2n_r + 1 \quad (21)$$

with off-diagonal coefficients given by (18-19). We remark by passing that these equations differ from those given in²² by the "minus" sign near f_{n+1n} , but changing this sign to plus means merely redefinition of the base wave functions (every even base function acquires the opposite sign) and does not affect the energy spectrum.

By the numerical diagonalization of the system (20-21) we obtain the band energy spectrum as function of α (we calculated n up to ~ 1200), as well as corresponding wave functions. Fig.1 shows the samples of the energy spectrum for different $|j|$ ($= 1/2, 19/2, 255/2$). The sample wavefunctions of few excited states of (1) are shown on Figs. 2 and 3. Fig. 2 shows wave functions in phonon coordinate representation (in the plane $Q_1 \times Q_2$), while Fig. 3 uses the projection $|\langle \chi | \Phi_n^0 \rangle|^2$ on the unperturbed ($\alpha = 0$) states of radial oscillator (15)²³

One of the remarkable features of excited states in JT models (both symmetric and generalized) is the existence of strongly localized ("exotic"⁷) states emerging occasionally among more extended ones. These states are exemplified on both Fig. 2 ($n = 40$) and Fig.3 ($n = 58$ for $j = 19/2$). One can see that the state labeled $n = 40$ on Fig.2 even has the dispersion smaller than that of the ground state $n = 1$ which peculiarity seems to have given

them such a name⁹. There is a relation between the position of localized states and spectral picture of levels (Fig.1). The spectrum of Fig.1 shows two sets of "diabatic" levels² (directed up- and downwards) which reflect different behavior of the two main wells of the effective potential¹⁵ with changing α . The exotic states appear to pertain to the directed upwards diabatic lines of the spectrum seen markedly on Fig. 1, b,c.

The multitude of avoided crossings (and therefore the domain referred to as "quantum chaotic") is thus formed in the intermediate energy region where these two "phases" coexist, that is above the first (lowest) "diabatic line". It is clearly seen on Figs. 1, b,c, that is at big values of angular momentum number j , while for small values of j these exotic states, while still exist, but do not come into complex interplay with ordered states. This picture is in agreement with the semiclassical treatment of the problem (see below) where the classically chaotic region is shown to emerge sharply above some critical energy E_c .

III. ANALYTICAL QUANTUM TREATMENT

A. Strong-coupling approximation. “Exotic” states

The peculiarities of the spectra shown in Fig. 1 as well as their connection to the character of pertaining wavefunctions (Figs. 2 and 3) can be understood from merely a rough approximation to the set of equations (20-21) in the following way. For $|j| \gg n_r$ there holds from (18)-(19) $f_{n_r, n_r} \gg |f_{n_r+1, n_r}|$ and the basis functions in (20-21) appear to be “clustered” in the sense that the coefficients c_{2n_r}, c_{2n_r+1} pertaining to the same n_r are coupled together (through f_{n_r, n_r}) essentially stronger than to neighboring elements. Therefore, in the limiting case of $|j| \gg n_r$ the thus reduced version of (20-21) for each n_r gives us two localized solutions for the energy

$$E(\alpha) = 2n_r \pm \sqrt{2(n_r + 1 + |j - 1/2|)\alpha}, \quad n_r = 0, 1, \dots \quad (22)$$

with corresponding eigenvectors $c_{2n_r} = c_{2n_r+1}$ and $c_{2n_r} = -c_{2n_r+1}$, other c_n being zero.

It is seen from Fig. 1 a-c that the slopes of the corresponding lines follow surprisingly well the predictions given by (22). This is valid for several lower clusters with small n_r which emerge as markedly seen “adiabatic” lines (directed upwards). At higher n_r when $j \leq n_r$ the “inter-cluster” f_{n_r+1, n_r} and inside-cluster elements $|f_{n_r, n_r}|$ are of comparable magnitudes and the long-range correlations yield the solutions rather extended which is also seen on the upper parts of spectra in Figs. 1a,b.

If there were not at all intercluster interaction, the energy lines from different clusters would regularly cross. The avoided crossings result from non-vanishing intercluster interactions. We can take into account the intercluster elements as a perturbation to the “strong coupling solution”. The amendments are essential near the points of crossings of the unperturbed energies thus giving the splitting (avoided crossings). In the vicinity of the avoiding crossing we can approximately represent the relevant Hamiltonian as an effective (2×2) matrix in the form:

$$\hat{H} = \begin{pmatrix} p\tau & u \\ u & 0 \end{pmatrix} \quad (23)$$

where $\tau = \alpha - \alpha_0$ (α_0 is the point of level collision if there were no interaction), and p and u are some constants. The matrix (23) accounts for the collision of two levels - one lying at $E = 0$ (if $\tau = \pm\infty$) and other moving asymptotically with velocity p . In the representation (23) we are in the frame of reference moving downwards with α so that the velocity of the non-exotic levels is zero. If the colliding levels are weakly affected by neighbours we can consider p and u to be approximately constants. The minimal avoided crossing (at $\tau = 0$) is thus $2|u|$. Including other non-exotic levels (thus situated at distances $1, 2, \dots$) leads to the extension of the matrix (23) to the shape given by equation (2) of²⁴ and accounting for a single level moving with velocity p and crossing subsequently parallel energy levels y_1, y_2, \dots with effective interaction strengths u_1, u_2, \dots . It was shown there that for

equidistant energies y_i and equal strengths u_i this system immediately gives the solution in the shape of a soliton propagating (with pseudotime τ) through the “lattice” y_n with natural analytical predictions as to the shape of energy eigenvalues $x_n(\tau)$. This soliton-like solution corresponds to our adiabatic level. The parameter p equals to the relative slope of exotic (adiabatic) and ordinary level and can be estimated in the strong-coupling approximation using (22). For the first adiabatic line it therefore holds $p \simeq 2\sqrt{2j}$. In the same approximation, treating intercluster elements as perturbation we can find, for example, for the first avoided crossing of the lowest adiabatic line the estimation $u \sim 2/\sqrt{j}$. Next subsequent avoided crossings are not treatable in this approximation, since there is no intercluster interaction between clusters unless they are neighboring. To account for the avoided crossings along the adiabatic line we can use the approximation presented in the following subsection.

The formalism of generalized Calogero-Moser gas has been developed^{2,17,18} as a useful alternative approach for Hamiltonians of the type $H = H_0 + \alpha V$ (the perturbation term linearly dependent on α) by mapping the eigenvalue equations on a statistical many-body system of interacting pseudoparticles. There α is a controlling parameter considered as a pseudotime, $\alpha \equiv \tau$. The eigenvalues were defined as dynamic variables $E_n(\alpha) \equiv x_n(\tau)$, $dx_n/d\tau = p_n(\tau)$. Respective classical dynamic equations for the pseudoparticles evolving in the pseudotime τ are

$$\frac{dp_n}{d\tau} = 2 \sum_{m(\neq n)} \frac{L_{nm}L_{mn}}{(x_m - x_n)^3}$$

$$\frac{dL_{mn}}{d\tau} = \sum_{l(\neq(m,n))} L_{ml}L_{ln} \left[\frac{1}{(x_n - x_l)^2} - \frac{1}{(x_m - x_l)^2} \right] \quad (24)$$

where

$$p_n \equiv \langle n(\tau) | V | n(\tau) \rangle \equiv V_{nn},$$

$$L_{mn}(\tau) = (x_n(\tau) - x_m(\tau))V_{mn} = -L_{nm} \quad (25)$$

In our case from (18-19) we get (in what follows we simplify notation, $n \equiv n_r$)

$$L_{2n, 2n+1} = \sqrt{2}\sqrt{n+1+|j-1/2|} \cdot (x_{2n+1}(\tau) - x_{2n}(\tau)),$$

$$L_{2n-1, 2n} = -\sqrt{2}\sqrt{n+1} \cdot (x_{2n}(\tau) - x_{2n-1}(\tau)) \quad (26)$$

Dynamic equations for a pair of even and odd coupled trajectories are then

$$\frac{dp_{2n}}{d\tau} = 2 \frac{L_{2n, 2n+1} \cdot L_{2n+1, 2n}}{(x_{2n+1} - x_{2n})^3} + 2 \frac{L_{2n, 2n-1} \cdot L_{2n-1, 2n}}{(x_{2n-1} - x_{2n})^3}$$

$$\frac{dp_{2n+1}}{d\tau} = 2 \frac{L_{2n+1, 2n+2} \cdot L_{2n+2, 2n+1}}{(x_{2n+2} - x_{2n+1})^3} + 2 \frac{L_{2n+1, 2n} \cdot L_{2n, 2n+1}}{(x_{2n} - x_{2n+1})^3} \quad (27)$$

In what follows we define small fluctuation δ by $x_{2n+1} - x_{2n} \equiv 1 + \delta_{2n}$, and approximate $(x_{2n+1} - x_{2n})^{-1} \approx 1 - \delta_{2n} + \delta_{2n}^2 - \delta_{2n}^3$. From (26)–(27) we get nonlinear set of equations

$$\frac{\partial^2 \delta_{2n}}{\partial \tau^2} - v_1^2 (\delta_{2n+1} + \delta_{2n-1} - 2\delta_{2n}) = f - 4|j - \frac{1}{2}| (\delta_{2n+1} + \delta_{2n-1}) - 4\delta_{2n-1} - 4(n+1)(\delta_{2n+1}^2 - \delta_{2n+1}^3) - 4n(\delta_{2n-1}^2 - \delta_{2n-1}^3), \quad (28)$$

$$\frac{\partial^2 \delta_{2n+1}}{\partial \tau^2} - v_2^2 (\delta_{2n+2} + \delta_{2n} - 2\delta_{2n+1}) = -f + 4|j - \frac{1}{2}| (\delta_{2n} + \delta_{2n+2}) + 4\delta_{2n+2} - 4(\delta_{2n+2}^2 - \delta_{2n+2}^3) - 8|j - 1/2| (\delta_{2n+1}^2 - \delta_{2n+1}^3). \quad (29)$$

where $v_1^2 = 4(n+1 + |j - 1/2|)$, $v_2^2 = 4(n+1)$, $f = 4 + 8|j - 1/2|$.

For large $n \gg |j|$, $v_1^2 \approx v_2^2$, equations (28) and (29) exhibit wave-like character in n . In linear approximation the last of equations bears solution $\delta_{2n+1} \approx J_0(2\sqrt{|2j-1|n})$ ($J_0(z)$ is Bessel function), which can be recognized in the upper part of the spectra in Figs. 1a,b and in Figs. 4a,g. The level avoidings in this linear part are kinematical and lead to clustering (dimerization) visualized in level spacing probability distributions (Section V).

Equations (28) and (29) allow a useful insight into the effects of nonlinearities on the levels dynamics involved. Defining phase variable $\zeta = n - v\tau$ one obtains

for $\bar{\delta}_{2n+1} = \delta_{2n+1} - 1$ at $|j| \gg n$:

$$-(v^2 - 4|j|) \frac{\partial^2 \bar{\delta}_{2n+1}}{\partial \zeta^2} + 16|j| (\bar{\delta}_{2n+1} + \bar{\delta}_{2n+1}^2) \approx 0. \quad (30)$$

If $4|j| < v^2$, then

$$\delta_{2n+1} = 1 - \frac{3}{2} \cosh^{-2} \left(2 \frac{(4|j|)^{1/2}}{(v^2 - 4|j|)^{1/2}} (\zeta - \zeta_0) \right). \quad (31)$$

Then identifying $\frac{\partial x_{2n+1}}{\partial n} = 1 + \delta_{2n+1}$ we obtain a soliton shaped (kink) solution

$$x_{2n+1} = 2n - \frac{3}{4} \frac{(v^2 - 4|j|)^{1/2}}{(4|j|)^{1/2}} \tanh \left(2 \frac{(4|j|)^{1/2}}{(v^2 - 4|j|)^{1/2}} (\zeta - \zeta_0) \right), \quad \zeta - \zeta_0 = n - n_0 - v(\tau - \tau_0), \quad (32)$$

corresponding to the tunnelling between two subsequent levels of opposite parity. There, many true dynamical level avoidings result in the system of *kink trains* between subsequent pairs of levels. The limiting velocity corresponding to the limit of vanishing fluctuation δ_{2n+1} and thus also vanishing of the tunnelling.

In equation (29) for δ_{2n} we take $\delta_{2n} = \bar{\delta}_{2n} + x$, therefore choosing x so as to eliminate the quadratic terms in (28). Let us take approximately $\delta_{2n+1} \approx \delta_{2n-1} \approx -\delta_{2n}$. Then we arrive at equation

$$\frac{1}{4} \frac{\partial^2 \bar{\delta}_{2n}}{\partial \tau^2} - n \frac{\partial^2 \bar{\delta}_{2n}}{\partial n^2} - \left(\frac{2}{3}n - 2|j| \right) \bar{\delta}_{2n} + 2n \bar{\delta}_{2n}^3 = \frac{4}{3}(2j - n/9). \quad (33)$$

If the oscillations in n can be neglected, under conditions $B \equiv 2n/3 - 2|j| > 0$ and $F \equiv \frac{4}{3}(2j - n/9) > 0$ (or $n > 2|j| > \frac{2n}{18}$), the solution exists of periodic nonsinusoidal shape which is spanned by F (nucleation fluctuation). With increasing j the energy of the nucleus grows until the kink generates. Respective solution reads

$$\bar{\delta}_{2n} = a \frac{n_1 + \cos(2v\tau)}{n_2 + \cos(2v\tau)}, \quad (34)$$

where a, b, n_1, n_2 are given as²⁵

$$n_1 = (2 - n_2^2)/n_2, \quad a^2 = \frac{B}{2n} \frac{n_2^2}{2 + n_2^2}, \quad 4v^2 = 2B \frac{n_2^2 - 1}{n_2^2 + 2}, \quad a = -\frac{F}{2B} (2 + n_2^2). \quad (35)$$

From equation $F = a(2na^2 - B)$ it is evident that the am-

plitude a of the fluctuation $\bar{\delta}_{2n}$ is spanned by the driving

field F , growing with $|j|$ until the energy of the fluctuation reaches the energy of the kink.

B. Weak-coupling approximation

This is the case opposite to the previous one, and valid for $j \ll n_r$. Rewrite the system (20-21) with coefficients

$f_{nn} = \sqrt{2}\sqrt{n+1+|j-1/2|}$, $f_{n+1n} = \sqrt{2}\sqrt{n+1}$ identically in the following way (here we again simplify labelling by n instead of n_r):

$$\begin{cases} C_{2n}(E_{2n}^0 - E) + \alpha [C_{2n+1}\sqrt{2n+1} + C_{2n}\sqrt{2n}] + \alpha C_{2n+1}k_n = 0, \\ C_{2n+1}(E_{2n+1}^0 - E) + \alpha [C_{2n}\sqrt{2n+1} + C_{2n+2}\sqrt{2n+2}] + \alpha C_{2n}k_n = 0 \end{cases} \quad (36)$$

with

$$k_n \equiv \sqrt{2n+1} \left(\sqrt{1 + \frac{2j}{2n+1}} - 1 \right), \quad n = 0, 1, \dots \quad (37)$$

($k_n \sim j/\sqrt{2n+1} \ll 1$ if $j \ll n$).

Then the whole system (36) is elegantly cast as $\hat{H}\Psi = E\Psi$ with

$$\hat{H} = \hat{b}^+\hat{b} + \alpha (\hat{b}^+ + \hat{b}) + \delta\hat{V} \equiv \hat{H}_0 + \delta\hat{V} \quad (38)$$

with *formal* notations: $C_{2n} \rightarrow |2n\rangle$, $C_{2n+1} \rightarrow |2n+1\rangle$ and operators \hat{b}^+ , \hat{b} acting upon our radial $|n\rangle$ as ordinary creation-annihilation operators; the “perturbation” $\delta\hat{V}$ acts under following recipe:

$$\delta\hat{V} = \alpha \cdot \begin{cases} 2n : & k_n C_{2n+1}, \\ 2n+1 : & k_n C_{2n}. \end{cases} \quad (39)$$

From there we immediately get the solution of the “unperturbed” problem $H_0\psi = E_0\psi$ in terms of the displaced Fock states (by acting the “coherent” operator $D(\gamma) \equiv \exp(\gamma(\hat{b}^+ - \hat{b}))$ on our pseudostates):

$$|\Psi\rangle \equiv |\tilde{n}\rangle = D(-\alpha)|n\rangle \quad (40)$$

with “unperturbed” energies $E_n^{(0)} = n - \alpha^2$.

From the above it is reasonable to investigate the reduced spectrum from which the “secular parts” of energies are subtracted: $\delta x_n \equiv E_n - n + \alpha^2 - (j - 1/2)$ (see Fig. 4). It is clear that within applicability of the perturbation treatment the deviations δx_n are confined between $(-0.5, +0.5)$. From our calculations it followed that this assertion holds excellently for all energy levels lying *above the first (lowest) diabatic line*.

On the left-hand side of Fig. 4 we plotted the reduced wavelike spectrum δx_n as function of n for typical values of α, j . Examining Fig. 4 we observe that extracting secular part reveals rather interesting patterns which have not been noticed on the normal scale of the wavelike spectrum. The most striking peculiarity is thus a crossover from two twisting quasi-sinusoids for big n (and/or small α) to the pictures which curiously resemble chaotic intermittent patterns containing rather characteristic windows of regular motion. The cut-offs on the left parts of the spectra (small n) correspond to first diabatic line below which such a reduction loses sense (since the “perturbation” $\delta\hat{V}$ can no more be considered small compared to H_0).

We can proceed further in treating the problem (38) by means of the standard perturbation scheme in the base $|\tilde{m}\rangle$ (40). For further references useful quantities $\langle n|\tilde{m}\rangle \equiv \langle n|D(\beta)|m\rangle$ are required which can be calculated directly:

$$\begin{aligned} \langle n|D(\beta)|m\rangle &= \frac{1}{\sqrt{m!n!}} e^{-\beta^2/2} \cdot \frac{\partial^m}{\partial \lambda^m} [e^{-\lambda\beta}(\lambda + \beta)^n]_{\lambda=0} = \\ &= \exp\left(-\frac{\beta^2}{2}\right) \beta^{|n-m|} \cdot \frac{\sqrt{n!m!} \text{sign}(n-m)^{|n-m|}}{\min(n,m)!|n-m|!} \times {}_1F_1(-\min(n,m), 1 + |n-m|, \beta^2) = \\ &= \exp\left(-\frac{\beta^2}{2}\right) \beta^{|n-m|} \cdot \sqrt{\frac{m!}{n!}} L_m^{|n-m|}(\beta), \end{aligned} \quad (41)$$

where $L_m^{|n-m|}(\beta)$ are Laguerre polynomials.

Following properties of (41) are checked directly:

1. $\langle n|D(\beta)|m\rangle = \langle m|D(-\beta)|n\rangle$;
2. $\langle n|D(\beta)|n\rangle = \exp\left(-\frac{\beta^2}{2}\right) F_1(-n, 1, \beta^2)$;
3. $\langle n|D(\beta)|0\rangle \equiv \langle n|\beta\rangle = e^{-\frac{\beta^2}{2}} \frac{\beta^2}{\sqrt{n!}}$ (a common result for the coherent state projection over a Fock state).

Up to the first perturbation order the spectral energies thus read as (notation \tilde{n} merely reminds the fact that the

base functions are now “displaced Fock states” (40) not to be confused with $|n\rangle$)

$$E_{\tilde{n}} = \tilde{n} - \alpha^2 + \delta V_{\tilde{n}\tilde{n}} + \dots \quad (42)$$

with

$$\delta V_{\tilde{n}\tilde{n}} = \sum_{h,s} \langle \tilde{n}|h\rangle \langle h|\delta\hat{V}|s\rangle \langle s|\tilde{n}\rangle = \alpha \sum_{h=0}^{\infty} 2 \cdot \langle 2h+1|D(-\alpha)|n\rangle \cdot \langle 2h|D(-\alpha)|n\rangle \cdot k_h \quad (43)$$

(k_n defined in (37)).

In the scope of the present paper we do not present further detailed analysis of (43). We just mention now that from our numerical findings it follows that (43) gives essentially the same structure as presented in Fig. 4. Moreover, it can be used even for the ground state (lowest energy for given j) giving plausible fitting for very small and very big α , although serious discrepancies occur for $\alpha \sim \Omega$ rendering it absolutely unsatisfactory in this region.

IV. QUASICLASSICAL APPROXIMATION

In what follows we consider the properties of the semiclassical analogue of the generalized JT model. The “semiclassical” description of the quantum JT problem is obtained if we pass to the real Bloch variables^{3,5} related to pseudospin Pauli matrices

$$x(t) := \langle \sigma_x \rangle_t \quad y(t) := \langle \sigma_y \rangle_t \quad z(t) := \langle \sigma_z \rangle_t \quad (44)$$

and perform the decoupling of the oscillator (vibron) and electron variables within the framework of Born-Oppenheimer approximation. The resulting coupled set of the equations of motion reads as

$$\begin{aligned} \dot{x} &= -\alpha Q_1 y \\ \dot{y} &= \alpha Q_1 x + \beta Q_2 z \\ \dot{z} &= -\beta Q_2 y \end{aligned} \quad (45)$$

$$\begin{aligned} \dot{Q}_1 &= P_1, \quad \dot{Q}_2 = P_2 \\ \dot{P}_1 &= -Q_1 - \alpha z \\ \dot{P}_2 &= -Q_2 + \beta x. \end{aligned} \quad (46)$$

Essential integrals of motions are the norm on the unit Bloch sphere

$$x(t)^2 + y(t)^2 + z(t)^2 = 1 \quad (47)$$

and conservation of full energy

$$E = \frac{1}{2} (P_1^2 + Q_1^2 + P_2^2 + Q_2^2) + \alpha Q_1 z - \beta Q_2 x \quad (48)$$

(Note that the semiclassical equations of motions (45-46) can be directly obtained from the classical Hamiltonian (48)).

Further, we introduce the classical angular momentum

$$J \equiv Q_1 P_2 - Q_2 P_1 - y \quad (49)$$

which evolves according to

$$\frac{dJ}{dt} = (\alpha - \beta)(Q_2 z - Q_1 x) \quad (50)$$

that is in the case $\alpha = \beta$ momentum is a conserved quality, likewise it was in the quantum case. The system acquires then four degrees of freedom and, as we show, exhibits chaotic behavior in a certain range of parameters.

Strictly speaking, the way to passing to semiclassical approximation is on no account unique and presents essential ambiguity leaning upon different ways of decoupling³. We could equally start from the Foulton-Gouterman transformed model (however this transcription is more adequate for nonsymmetric case). Another possibility is merely the generalization of the scheme used by including higher-order momenta. Moreover, different ways of semiclassical approximation are known to lead to different answer concerning chaotic behavior of the system. We emphasize that such ambiguity simply means that the classical analogue of such a model is not well-defined and cannot be a primary object in exploring the quantum chaos issues. Traditionally the term “quantum chaos” is used to denote the traces of *classical* chaotic behavior on quantum level. Such considerations impose

additional vagueness to the mere concept of quantum chaotic studies.

Numerical integration of the system (45-46) shows that the system generally exhibits chaotic behavior (see sample trajectories on Fig.5), which is a common thing when one deals with two subsystems, one of which is treated classically (phonon subsystem in our case), and the other remains quantum. The domain of chaotic behavior lies however in the intermediate range of energies, which is remarkably seen from the frequency analysis of a sample trajectory in Fig. 6. Here we showed the Fourier spectrum of the Q_1 coordinate for different values of the total energy in a system (value of (48)), but the results for other coordinates are similar. We presented the simplest criterion to discriminate between regular and chaotic trajectories, but our analysis of Lyapunov exponents support these statements as well. Thus the phase picture (the lines of chaotic and regular domains in the plane $E - \alpha$) appears to be similar to analogous pictures known, for example, from the semiclassical treatment of spin systems²⁰. One more characteristic feature of the system is very sharp crossover (with increasing energy) between regular and nonregular behaviour at lower edge of chaotic spectrum; such a crossover apparently is manifested at quantum level as reaching the lowest diabatic line and thus entering the domain of multiple avoided crossings. However, one may notice that the chaotic domain is not always stretched over the whole phase space and it is possible to trace the narrow domains of regular behavior (i.e. KAM-tori) which separate different chaotic domains. In Fig. 5 we exemplified the existence of such a separatrix giving sample trajectories of z coordinate with different initial points on the phase plane. Namely, we choose initial point in the (x, y, z) subspace such that $x = \cos j\pi/40, y = 0, z = \sin j\pi/40, j = 1, 2, 3, \dots, 40$ and observed the trajectories of regular behavior for some particular j . For example, note the contrast of the trajectory behavior in Fig. 6b for $j=30$ and neighbour point $j = 31$ in Fig. 6c). Such traces of regular behavior in generically chaotic classical systems are conjectured⁶ to have their counterpart in the existence of the strongly localized exotic quantum states.

V. LEVEL STATISTICS

Statistical methods of investigation of the complex spectra are based on evaluation of various "chaoticity degrees" of quantum systems, i.e., the density of levels, distribution of nearest neighbour spacings (NNS), statistics of distribution of "curvatures" accounting for avoided crossings as well as more complicated measures of distribution of avoided crossings^{18,26,27}. Most of these characteristics can be obtained within the framework of random-matrix theory (RMT)^{26,28,29,30}, whose predictions are supposed to adequately describe the quantum systems with generically chaotic classical analogues. However, the predictions of RMT cover in a satisfactory

fashion only the "chaotic" limit of these systems, classifying them into three universality classes according to the time-reversibility of the underlying Hamiltonian^{26,28,30} (that is Gaussian orthogonal GOE, unitary GUE and symplectic GSE ensembles). The fourth "universality class" corresponds however to rather regular dynamics (for example, if the classical analogue of the system for some values of controlling parameters exhibit mostly regular KAM trajectories).

In recent years however there came an understanding that chaotic patterns are to be sought not only from the energy level distribution themselves but rather from the pictures of their changing with the change of controlling parameters in Hamiltonian (α). Thus, an alternative statistical approach is based on the concept of fully integrable description of the spectra by the dynamical model of Calogero-Moser gas of interacting (repulsing) pseudoparticles^{17,18} where the controlling parameter is considered a pseudotime (Section III).

The dynamical equations for the eigenfunctions $|x(\tau)\rangle$ of this Hamiltonian bring, for example, to the notion of level curvature $\ddot{x}(\tau)$ ^{18,27} and several conjectures about its relation to the nature of underlying RMT ensemble. The various characteristics of level curvature distributions were reported as handy indicators of quantum chaos traces in a system. In particular, it was suggested²⁰ that for energy regions with quantum chaos holds the scaling $\Delta K \sim j^\nu$ with positive ν , meanwhile for non-chaotic regions ν is rather negative or close to zero. We investigated (Fig.7) the widths ΔK of the distributions of level curvatures $P(K)$ displayed as functions of j for a set of α . The level statistics of Fig. 7 (and of the following Fig. 8) was taken from the energy intervals above the first "diabatic" line where multiple avoided crossings first come into being. For improvement of statistics we used the standard recipe of collecting the level sequences from a number of α values lying in the neighborhood. The figure 7 markedly shows the scaling behavior $\Delta K \sim j^\nu$ with the scaling coefficient $\nu \in (0.99 - 1.01)$ for all α .

The statistical investigation of the level spacings in symmetric JT case for separate j does not bring us to a rich world. Indeed, the realm of the symmetric model with definite j is that of effectively two-dimensional oscillator (or rather two oscillators pertaining to two electron levels). The unperturbed $\alpha = 0$ problem is thus trivial: all levels of a quantum harmonic oscillator are equidistant, so $P(S) = \delta(S - 1)$. The nontrivial behavior appears to be consequence of effective coupling two oscillators through α . In Fig. 7 we show the level spacing distributions $P(S)$ for a set of j with different α .

Our results indicate that the most close to RMT prediction situations (RMT would yield Wigner distribution of NNS in the form $P(S) \sim S \exp(-S^2)$) are located at intermediate values of j and α as it is seen for pictures with $j = 19/2$. Meanwhile the extreme values of j and α do not fit RMT theory at all. However one can notice a crossover between two distinctly different types of behavior for (seen, for example, at $j = 5/2$ and

$j = 255/2$). Such a behavior can be semi-quantitatively explained basing on the conception of effective potential wells, for example, built on the semiclassical coherent “probe” function in the space of their parameters (see¹⁵). Namely, characteristic for big j is the presence of two almost noninteracting wells (which is markedly seen from Fig. 4 containing spectral entropies). We can assume that each of the well refers to a separate quantum oscillator having level spacing a and b (let $a < b$). Consider a problem of finding a superposition of distributions of two sets of levels with $P_1(S) = \delta(S-a)$, $P_2(S) = \delta(S-b)$ each provided that they are *independent*. Repeating simple probabilistic considerations for this case (see for details, e.g.³¹), we find that the cumulative level distribution is of the form:

$$P(S) \simeq \frac{2}{b}\theta(a-S) + \delta(S-a), \quad (51)$$

θ being step function (we considered $a \ll b$; if they are comparable, a refinement to (51) is straightforward). The striking conformity of Fig. 8 to the prediction (51) with $a \simeq 1.7$ and $b = 4$ for big j and α (see $j = 255/2$, $\alpha \geq 5$) is perceivable. From the “adiabatic sheet” treatment in¹⁵ we can even define the parameters of both effective potential wells. The opposite case of small j (α) apparently indicates dimerized structure with two dominating spacings, with increasing extent of correlation when decreasing j and α .

The level spacing statistics taken separately for particular values of j is the base of more realistic investigation of the level statistics of the whole spectrum of the system whose Hamiltonian in this representation is a block matrix of blocks on the diagonal corresponding to definite j and off-diagonal blocks coupling (in generalized $E \otimes (b_1 + b_2)$ JT model) for different j 's. The peculiarity of the symmetric Jahn-Teller case is that the interblock coupling is exactly zero, and, as it was shown already in³² with a variant of the central limit theorem, the superposition of (infinite or very large number) independent blocks will give the cumulative distribution which must be of Poissonian character, $P(S) = \exp(-S)$. This result is exactly that obtained by Yamasaki et al¹³ for the absence of (trigonal) nonlinearity and which was claimed to testimony of the absence of any traces of quantum chaos in this case. The detailed account for the level statistics for the generalised JT model including the symmetric JT case as its partial case will be reported by us elsewhere. For the sake of the present paper we just mention the serious deviations of the expected Poisson result in the symmetric case in the domain of dominating quantum fluctuations ($\Omega > (\alpha, \beta)$). Indeed, the $P(S)$ distribution shown for $\alpha = \beta = 0.5$ exhibits considerable deviations from the expected Poisson case showing anomalously large variance > 4 (for $\alpha = \beta = 1$ this dispersion is $\simeq 1.17$, and for the domain $\Omega < \alpha$ it is rather rigid falling normally within $0.7 - 0.8$ irrespectively to the values of α). These anomalies are apparently due to

the high non-uniformity of the spectral statistics in this case for different energy intervals. In Fig. 9 we showed the level spacing distributions for the case $\alpha = \beta = 0.5$ taken for separate level intervals (100 – 500, 500 – 1000, 1000 – 1500 and 1500 – 2000) from which this difference is apparent. The distributions with $\alpha, \beta > 1$, in the contrast, are rather robust with respect to changing energy intervals.

VI. CONCLUSION

Energy spectrum of a long but finite chain of correlated clusters is governed by interplay of intra- and intercluster interactions (repulsions) determined by two quantum numbers, rotational j and radial n_r . At small coupling $\alpha < \Omega$ and small $|j|$, $|j| \ll n_r$, the excited spectrum is long-range ordered and the broad *dimerized region* is a sample of pairwise oscillating levels. The level avoidings (upper part of spectra in Figs. 1 b,c) are due to the competition of comparable intercluster and intracluster interactions. In a strong coupling limit, $\alpha > \Omega$, large j , $|j| \gg n_r$ (the intercluster interaction is negligible when compared to the intracluster one) there appears a *kink lattice*, a regular lattice of clusters of levels. Here the levels are connected by a flip (kink) up to higher level of opposite parity due to the tunnelling between the levels (Fig. 1c,d above the diabatic line). At moderate $|j|$ and α there appears a medium region of strong *nonlinear fluctuations responsible for nucleation of the kinks* (Figs. 1b, 4d,e,f)).

From the other hand, qualitative features of the excited spectra of $E \otimes e$ Jahn-Teller model can be understood from the outline of the shape of the effective potential used for investigating the ground state of the model^{15,33}. With increase of j and α up to the semiclassical limit there emerge up to three effective potential minima. In accordance with this we identify the above mentioned three phases in the spectra: for small coupling α the dimerized phase is related to two broad minima of the potential. Increasing α there appears one additional narrow minimum (for the ground state its counterpart was responsible for emerging the “tunneling phase” or light polaron³³). The complex interplay of wavefunctions located over three minima corresponds to our intermediate region (Figs. 4d,f) where the level statistics (Fig. 8) exhibits patterns close to those expected for fully chaotic RMT statistics²⁸. Next, subsequent increasing α (and j) brings to the suppression of initial “weak coupling” wide minimum in the semiclassical limit of large α . Thus there persist two almost non-interacting potential wells - a narrow and a wide one. The two remaining noninteracting branches of spectra are markedly seen on Fig. 4,j. The lowest branch of the spectral entropy (Fig.4f) is related to the (third) narrow minimum of the effective potential responsible for the kink lattice phase of avoided crossings (localized states) in energy spectra. This behavior is also supported by the shape of the level spacing distri-

bution (Fig. 8,d) and (51)) which has marked character of superimposing of two almost non-interacting effective oscillators with different frequencies.

In a semiclassical approximation (Section IV) the middle part of the energy spectra is characterized by pronounced chaotic behaviour of trajectories with randomly distributed frequencies (Fig.6) and positive Lyapunov exponents. Characteristic for this region in the phase plane is sharp transition from regularity to chaos at its lower edge and existence of separatrices between ordered and chaotic patterns inside (Fig.5).

Statistical level spacing probability distributions investigated in Section V were numerically calculated for particular j 's. They are shown to exhibit up to three maxima (Fig.8) depending on j and α . For moderate j and α a pair of almost symmetric prominent peaks of $P(s)$ are related to two dominating strongly correlated potential wells which are getting closer at small α and j (Fig. 8). Two dominating peaks of level spacings refer to dimerization clustering of subsequent levels with opposite parity. At large j and α (quasiclassical limit) the probability distributions strictly follow the shape of the ground state effective potential (Fig.8d). Analysis of cumulative statistical distributions of level spacings shows strongly changing picture of different segments of spectra especially at weak couplings (Fig.9). The dimerized phase is pronounced in the lowest part of spectra where a strong clustering is apparent from two peaks of the level spacing distribution $P(s)$. In the middle part of spectra

some patterns of Wigner distribution at least at large s are perceivable. The widths of level curvature distributions were found (Fig.7) to be scaled as $\Delta K \propto j^\nu$, $\nu \propto 1$ and thus satisfying the criterion suggested²⁰ for indicating chaotic patterns in our quantum system.

The levels with $j \neq j'$ are uncorrelated (matrix elements between the states are zero) and the respective levels thus intersect (Section II). The cumulative level spacing probability distributions (Fig.9) consist of contributions of all j 's: Respective Poissonian distributions superimpose the above described partial distributions. The cumulative level spacing distributions exhibit enormously large dispersions $\gg 1$ which can be an evidence for overlapping of distributions of two kinds: Poissonian one from the crossing of uncorrelated levels $j \neq j'$ and the two-peak ones for particular j -s described above. In the quasiclassical limit $j \rightarrow \infty$ the spectrum tends to continuum and respective levels at $j \rightarrow j'$ will tend to avoiding.

Acknowledgement. We thank Prof. J. Peřina for useful discussion. Great acknowledge for financial support of the project No. 1/0251/05 is to the Grant Agency VEGA, Bratislava. One of us (S.Sh.) is also indebted for the partial support by the project No. LN00A015 of the Ministry of Education of the Czech Republic as well as for a financial support by the Department of Theoretical Physics of the Faculty of Science of Palacký University in Olomouc.

-
- ¹ B. Eckhardt, Phys. Rep. **163**, 205 (1988).
² K. Nakamura, Quantum Chaos-A New Paradigm of Non-linear Dynamics (Cambridge University Press, Cambridge, 1993).
³ R. Graham and M. Hörnerbach, Z. Phys. B **57**, 233 (1984), R. Graham and M. Hörnerbach, Phys. Lett. 101A, 61 (1984).
⁴ J. Eidson, R. F. Fox, Phys. Rev. **A 34**, 3288 (1986); R. F. Fox, J.C. Eidson, *ibid.*, **34**, 482 (1986); R. F. Fox, J. C. Eidson, *ibid.*, **36**, 4321 (1987).
⁵ R. Blümel, B. Esser, Phys. Rev. Lett. **72**, 3658 (1994); B. Esser, H. Schanz, Z. Phys. **B 96**, 553, (1995); H. Schanz, B. Esser, Z. Phys. **B 101**, 299 (1996); H. Schanz, B. Esser, Phys. Rev. **A 55**, 3375 (1997).
⁶ M.S. Santhanam, V.B. Sheorey, and A. Lakshminarayan, Phys. Rev. **E 57**, 345 (1998).
⁷ H. Eiermann, and M. Wagner, J. Chem. Phys. **96**, 4509 (1992).
⁸ U. Herfort, M. Wagner, J. Phys. Condens. Matter **13**, 3297 (2001).
⁹ A. Königter and M. Wagner, J. Chem. Phys. **92**, 4003 (1990).
¹⁰ P.W. Milloni, J.R. Ackerhalt, and H.W. Galbraith, Phys. Rev. Lett. **50** 966 (1983).
¹¹ K. Furuya, M.C. Nernes and G.Q. Pellegrino, Phys. Rev. Lett. **80** 5524 (1998).
¹² M. V. Berry and M. Tabor, Proc. Roy. Soc. London **356**, 375 (1977).
¹³ H. Yamasaki, Y. Natsume, A. Terai, K. Nakamura, Phys. Rev. **E 68**, 0462011 (2003).
¹⁴ M.C.M. O'Brien, Proc. Roy. Soc.(London) **A281**, 323 (1964).
¹⁵ E. Majerníková and S. Shpyrko, J. Phys.: Condens. Matter **15**, 2137 (2003).
¹⁶ V. Bužek, M. Orszag, M. Roško, Phys.Rev.Lett. **94**, 163601 (2005).
¹⁷ P. Pechukas, Phys. Rev. Lett. **51**, 943 (1983); T. Yukawa, Phys. Lett. **A 116**, 227 (1986).
¹⁸ P. Gaspard, S.A. Rice, H.J.Mikeska, K. Nakamura, Phys.Rev.A **42**, 4015 (1990).
¹⁹ E. Majerníková and S. Shpyrko, to be published.
²⁰ K.Nakamura, Y.Nakahara, A.R.Bishop, Phys.Rev.Lett **54** 861 (1985); K. Nakamura, A.R. Bishop, Phys. Rev. **B33**, 1963 (1986).
²¹ H.B. Shore, and L.M. Sander, Phys. Rev. **B 7**, 4537 (1973)
²² H.C. Longuet-Higgins, U. Öpik, M.H.L. Pryce, Proc. Roy. Soc. London, Ser. **A244**, 1 (1958).
²³ note that the numeration of states for Fig.3 labels the states with given j , and for Fig.2 all states are labeled in ascending order in energy.
²⁴ P. Gaspard, S.A. Rice, K. Nakamura, Phys. Rev. Lett. **63** 930 (1989).
²⁵ P. Lal, Phys. Lett. **114A**, 410 (1986).
²⁶ T.A. Brody, J. Flores, J.B. French, P.A. Mello, A. Pandey, S.S.M. Wong, Rev. Mod. Phys. **53**, 385 (1981).

- ²⁷ J.Zakrzewski, M.Kuś, Phys.Rev.Lett. **67** 2749 (1991);
 J.Zakrzewski, D.Delande, Phys.Rev.E **47** 1650 (1993);
 J.Zakrzewski, D.Delande, M.Kuś, Phys.Rev.E **47** 1665 (1993).
²⁸ F.J.Dyson, J.Math.Phys. **3** 140, 157 and 166 (1962);
 F.J.Dyson, J.Math.Phys. **3** 1191, 1199 (1962)
²⁹ F.J.Dyson, J.Math.Phys. **13** 90 (1972)
³⁰ M.L.Mehta, Nuclear Physics **18** 395 (1960); M.L.Mehta,
 M.Gaudin, Nuclear Physics **18** 420 (1960); M.Gaudin, Nuclear
 Physics **25** 447 (1961).
³¹ M.V.Berry, M.Robnik, J.Phys.A **17** (1984) 2413.
³² N.Rosenzweig, C.E.Porter, Phys.Rev. **120**, 1968-1714 (1960)
³³ E.Majerníková, J. Riedel, S.Shpyrko, Phys.Rev.B **65**, 174005 (2002).

Figure Captions

Figure 1. Level picture as function of α in symmetric JT case for different j ; a)-c): $j = 1/2, 19/2, 255/2$ respectively. Insets represent details of Figs. 1b, 1c.

Figure 2. Wavefunctions for $n=1$ (ground state), 39, 40 (localized "exotic"), 42, $\alpha = \beta = 2$.

Figure 3. Projections of exact symmetric ($\beta = \alpha$) states on the harmonic oscillator base, $|\langle \chi | \Phi_n^0 \rangle|^2$.

Figure 4. Reduced energies (see text) and spectral entropies of wavefunctions for different couplings α and j .

Figure 5. The semiclassical trajectory z for different initial conditions. Note the existence of the separatrix in the phase plane (regular KAM-tori) which separates several domains of generically chaotic motion.

Figure 6. Frequency spectrum of the semiclassical Q_1 trajectories for different values of total energy.

Figure 7. The scaled widths of curvature distributions $\Delta K \equiv \langle \Delta^2 K \rangle$ as function of j for different α . The scaling law $\Delta K \sim j^\nu$ is remarkably seen.

Figure 8. Level spacing distributions for particular j . Dimerization clustering related to two dominating level spacings is evident.

Figure 9. Level spacing distributions for subsequent segments of cumulative energy spectrum for small $\alpha < 1$. Dimerization clustering peaks as remnants of the distributions in Fig. 8 are evident. The reference curves pertain to Wigner (full), semi-Poisson (dotted), and Poisson (dashed) distributions.

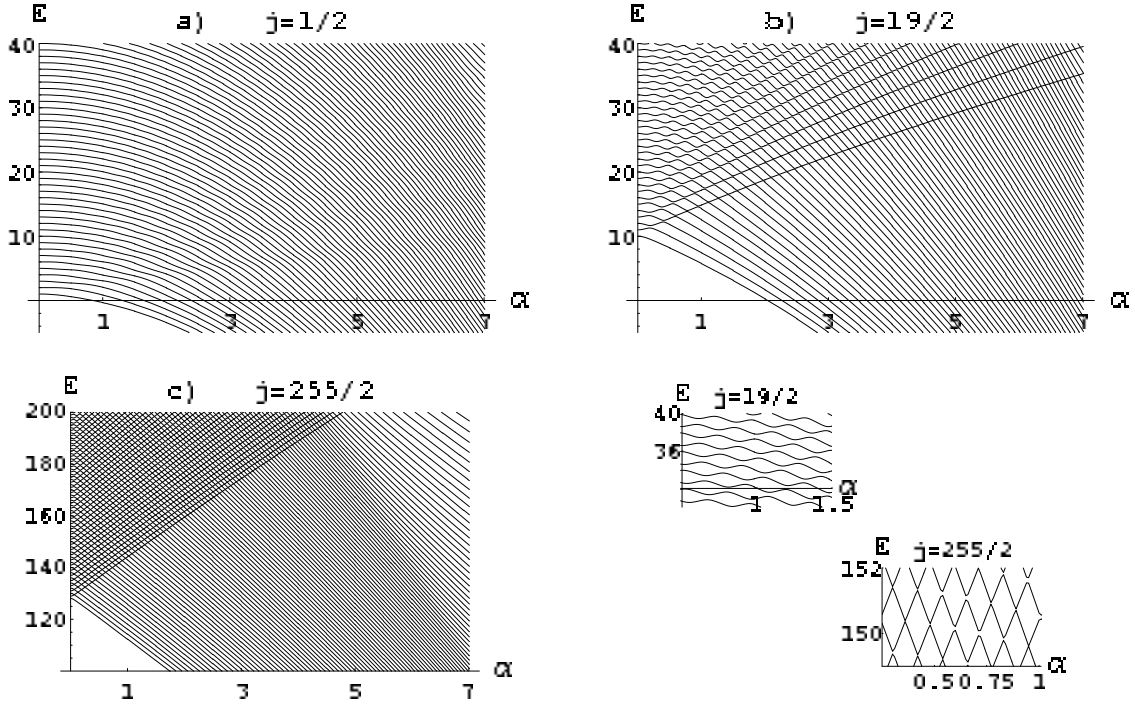


FIG. 1: Level picture as function of α in symmetric JT case for different j ; a)-c): $j = 1/2, 19/2, 255/2$ respectively. Insets represents details of Figs. 1b, 1c.

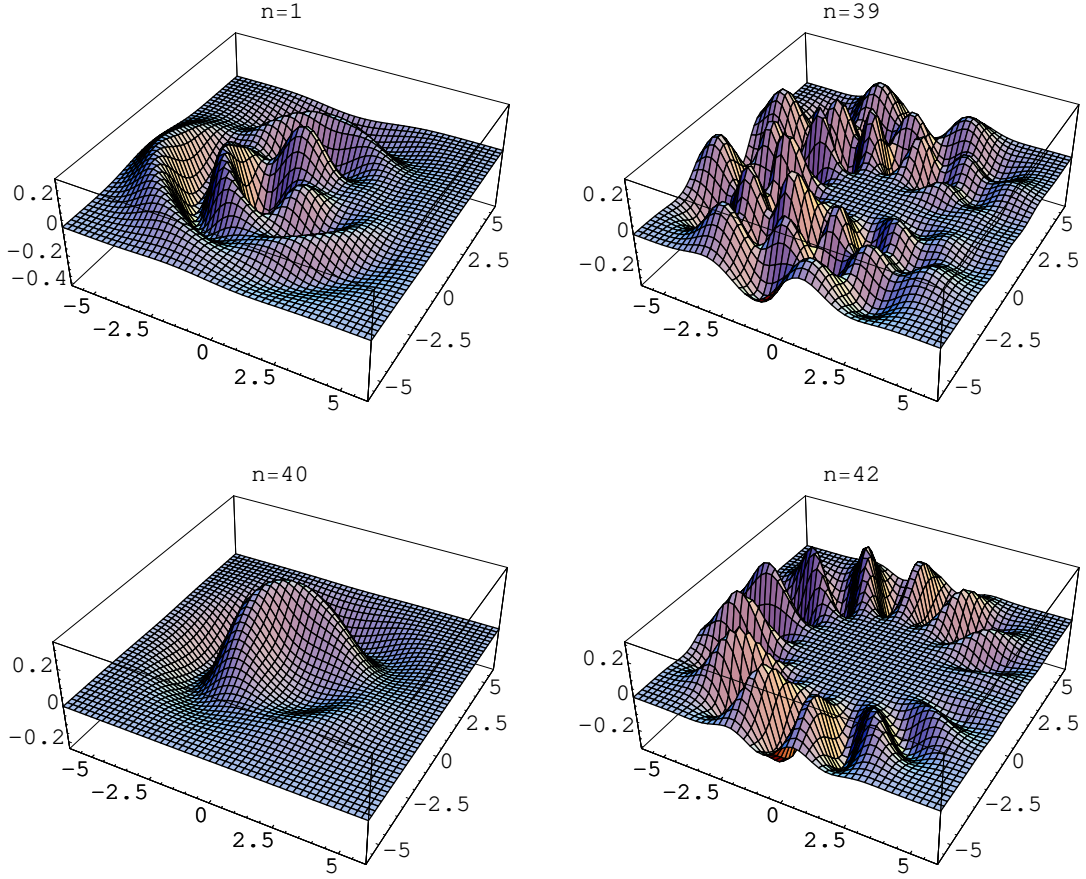
$\alpha=2 \quad \beta=2$ 

FIG. 2: Wavefunctions for $n=1$ (ground state), 39, 40 (localized "exotic"), 42, $\alpha = \beta = 2$.

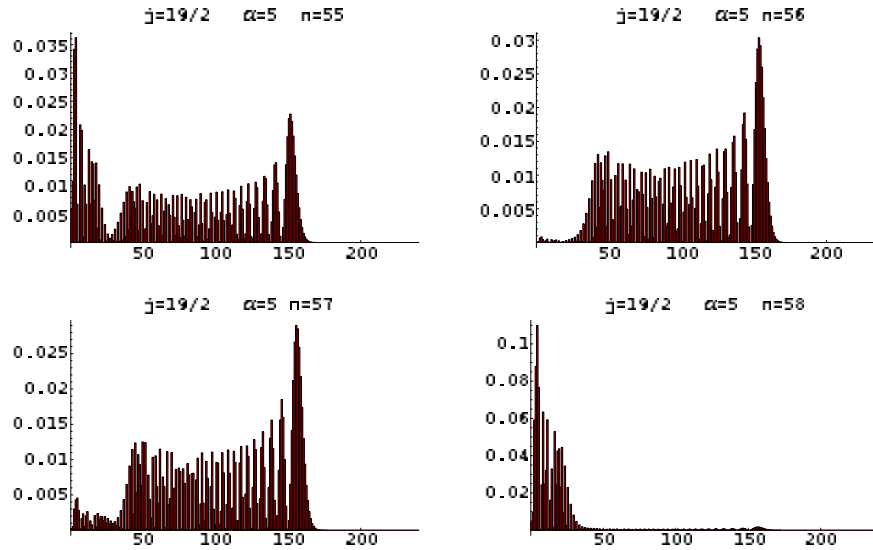


FIG. 3: Projections of exact symmetric ($\beta = \alpha$) states on the harmonic oscillator base, $|\langle \chi | \Phi_n^0 \rangle|^2$.

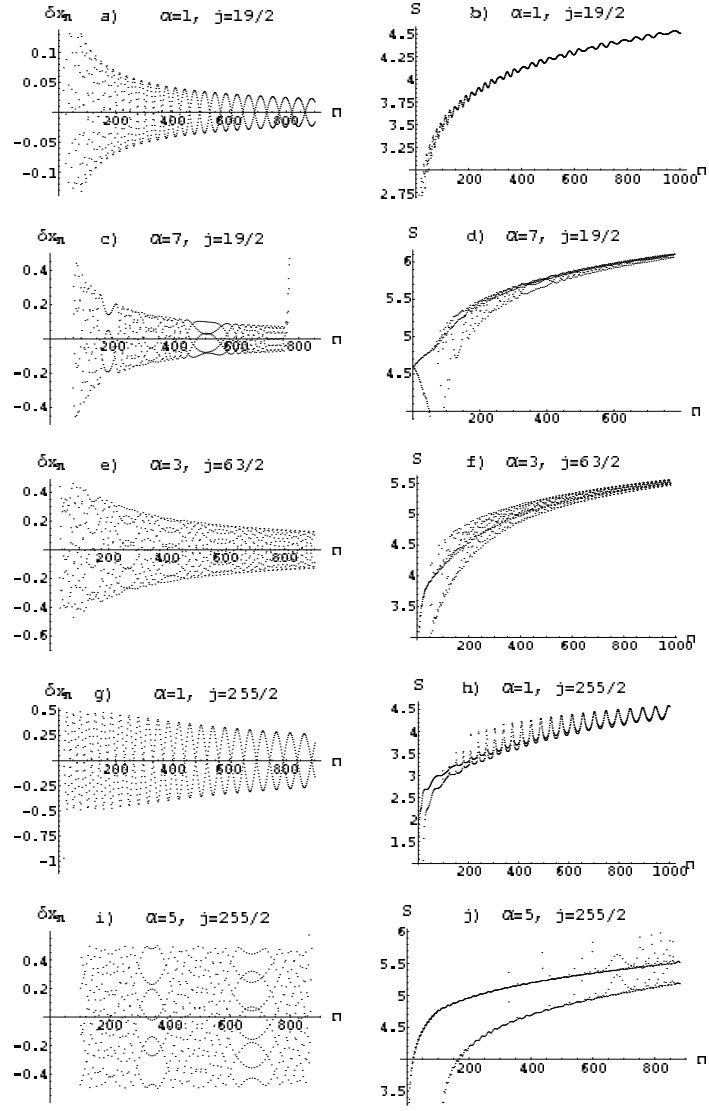


FIG. 4: Reduced energies (see text) and spectral entropies of wavefunctions for different couplings α and j .

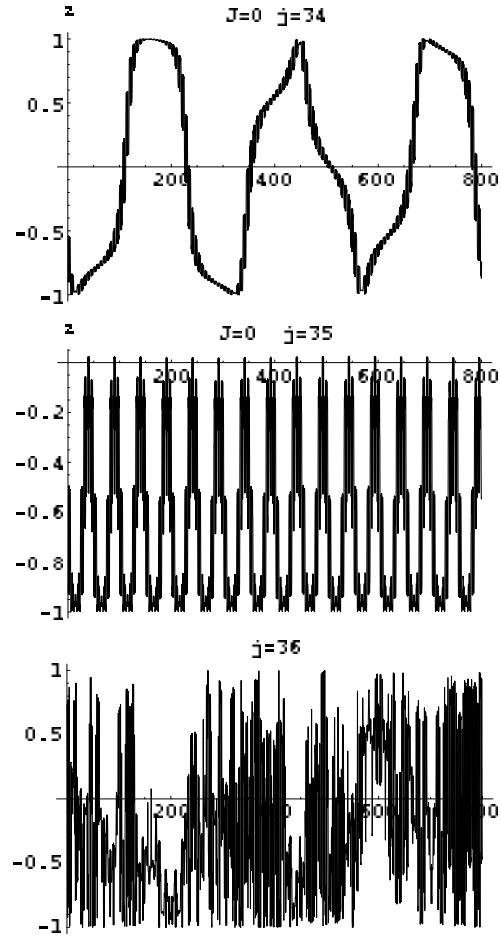


FIG. 5: The semiclassical trajectory z for different initial conditions. Note the existence of the separatrix in the phase plane (regular KAM-tori) which separates several domains of generically chaotic motion.

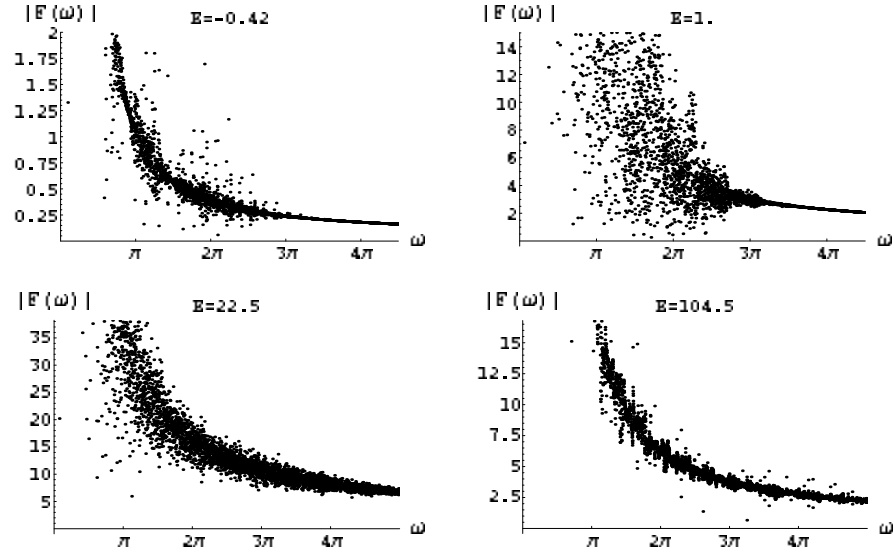


FIG. 6: Frequency spectrum of the semiclassical Q_1 trajectories for different values of total energy.

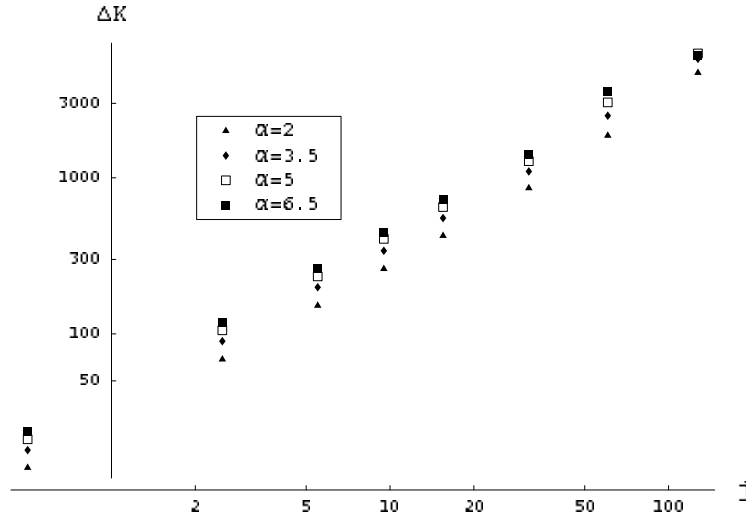


FIG. 7: The scaled widths of curvature distributions $\Delta K \equiv \langle \Delta^2 K \rangle$ as function of j for different α . The scaling law $\Delta K \sim j^\nu$ is remarkably seen.

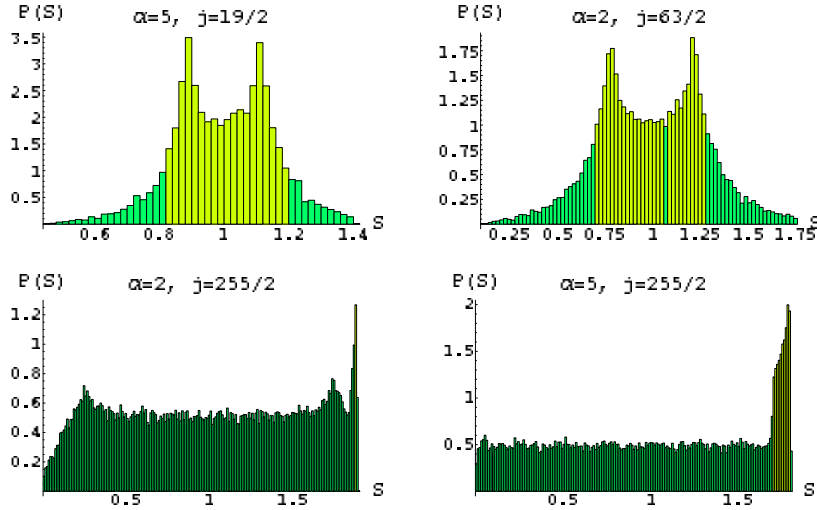


FIG. 8: Level spacing distributions for particular j . Dimerization clustering related to two dominating level spacings is evident.

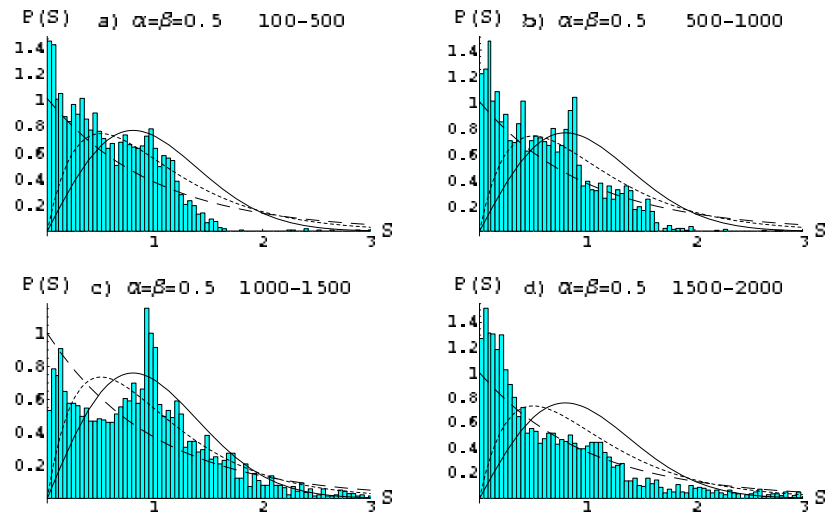


FIG. 9: Level spacing distributions for subsequent segments of cumulative energy spectrum for small $\alpha < 1$. Dimerization clustering peaks as remnants of the distribution in Fig. 8 are evident. The reference curves pertain to Wigner (full), semi-Poisson (dotted), and Poisson (dashed) distributions.